Model reduction applied to multi-stage assemblies of bladed disks

A. Sternchüss, E. Balmès
Laboratoire MSS-MAT, École Centrale Paris, UMR 8579,
Grande Voie des Vignes, 92295 Câtenay-Malabry Cedex, France
e-mail: **arnaud.sternchuss@ecp.fr**

P. Jean, J.-P. Lombard
Snecma (Safran Group)
Rond-point René Ravaud, 77550 Moissy-Cramayel Cedex, France

Abstract
This paper deals with model reduction of assemblies of bladed disks. Some considerations about the use of the Fourier theory to describe the dynamics of assemblies of geometrically periodic structures are first recalled. This allows to define a set of spatially mono-harmonic solutions that are used to build the kinematic subspaces in a subsequent reduction process. The main characteristics of this sector substructuring technique are then presented and discussed. Finally, the proposed methodology is applied to an industrial rotor provided by Snecma to demonstrate its capability to handle large finite element models.

1 Introduction

For a long time, the industrial practice has consisted in modelling separately each stage of the assembly of bladed disks that compose the rotor of a jet engine. In preliminary analyses, many simplifications are allowed by the nominal geometry of the individual stage when one exploits its properties of cyclic symmetry. Further analyses including mistuning or parametric modelling (rotation, temperature effects,...) can be carried out with more complex models. In both cases, a collection of reduction techniques has been proposed by many authors and many of them are currently used in the industrial design process of single stages [1, 2].

The current geometries of the disks make them more flexible, which leads to non-negligible coupling effects between stages [3, 4]. This inter-disk coupling controls the spread of the strain energy between disks and therefore is identified as the main cause of discrepancies between single stage and multi-stage dynamics. To minimize the modelling effort, the already existing mono-stage reduction techniques would be a good framework to deal with multi-stage assemblies. However, as underlined in [3], the critical point is the choice of the proper boundary conditions that would represent the inter-stage coupling. Recent work [4–6] has focused on multi-stage reduction procedures.

The first part of the present paper recalls the main characteristics of geometrically periodic structures. In particular, one focuses on the Fourier transform of the discrete fields that represent the motion. Multi-stage dynamics are derived from mono-disk dynamics, which allows to compute mono-harmonic eigensolutions, which are known to be modes for single disks.

In the second part, the methodology developed by the authors in [4, 7] is briefly recalled. This substructuring method consists in a decomposition of the disks into sector super-elements connected with each other through inter-sector elements and inter-disk ring elements. The kinematics of each sector super-element are sought

in a subspace generated by a set of targeted mono-harmonic modeshapes as defined by Laxalde *et al.* [6] and normal modes of the sector with its right and left interfaces fixed. The reduction leads to a very compact model whose assembly is straightforward and whose accuracy is driven by the choice of the reduction bases.

As an illustration, in the third part of the paper, the proposed method is applied to a realistic rotor model provided by Snecma. The exploitation of this model is not only the occasion to demonstrate that this methodology can be integrated in a industrial design process, but also to carry out performance tests (computing time, memory required for data storage, procedures of modeshape recovery, ...). A discussion about the content of the reduction bases is included in this section since the latter is critical in terms of model size and accuracy.

2 Multi-stage dynamics and cyclic symmetry

2.1 Fourier transform of geometrically periodic structures

A structure is said to present cyclic symmetry when it is composed of N_s geometrically identical angular sectors, numbered from 0 to $N_s - 1$, that are generated by rotations of a reference sector $\mathcal{S}^0$. When cyclic symmetry is preserved by the Ritz-Galerkin discretization process, the discrete displacement $\{q^s\}$ relative to the DOF set of sector $\mathcal{S}^s$ form a series $\{q\}^\top = \{\ q^0 \quad q^1 \quad \cdots \quad q^{N_s-1}\ \}$ whose Fourier transform can be computed. The discrete displacement $\{q\}$ is related to its Fourier harmonics stored in $\{\widehat{q}\}$ by the two matrix relations

$$\{\widehat{q}\} = [E^\top \otimes I_{N^0}]\ \{q\} \text{ and } \{q\} = [E \otimes I_{N^0}]\ \{\widehat{q}\}\,. \tag{1}$$

where $\{\widehat{q}\}^\top = \{\ \widehat{q}_0 \quad \cdots \quad \mathrm{Re}(\widehat{q}_\delta) \quad \mathrm{Im}(\widehat{q}_\delta) \quad \cdots \quad \widehat{q}_{\frac{N_s}{2}}\ \}$, $\otimes$ is the Kronecker product and I_{N^0} is the identity matrix of size the the number of DOFs in sector $\mathcal{S}^0$. The Fourier harmonics are real if $\delta = 0$ and $\delta = N_s/2$ (if N_s is even), complex otherwise. $[E]$ is the Fourier transform matrix defined by

$$[E] = \frac{1}{\sqrt{N_s}} \begin{bmatrix} 1 & \cdots & \sqrt{2} & 0 & \cdots & 1 \\ \vdots & & \vdots & \vdots & & \vdots \\ 1 & \cdots & \sqrt{2}\cos(\delta\,\alpha) & -\sqrt{2}\sin(\delta\,\alpha) & \cdots & -1 \\ \vdots & & \vdots & \vdots & & \vdots \\ 1 & \cdots & \sqrt{2}\cos(s\,\delta\,\alpha) & -\sqrt{2}\sin(s\,\delta\,\alpha) & \cdots & (-1)^s \\ \vdots & & \vdots & \vdots & & \vdots \\ 1 & \cdots & \sqrt{2}\cos((N_s-1)\,\delta\,\alpha) & -\sqrt{2}\sin((N_s-1)\,\delta\,\alpha) & \cdots & (-1)^{N_s-1} \end{bmatrix}. \tag{2}$$

When mechanical properties also satisfy cyclic symmetry, *i. e.* they are identical from sector to sector, any matrix $[A]$ defined on the full disk is recovered by $[A] = [I_{N_s} \otimes A^0]$, with $[A^0]$ the corresponding matrix in sector $\mathcal{S}^0$. The congruent transformation of matrix $[A]$, which corresponds to the expression of $[A]$ using DOFs $\{\widehat{q}\}$, is then

$$\begin{aligned} [\widehat{A}] &= \left[E^\top \otimes I_{N^0}\right] \left[I_{N_s} \otimes A^0\right] [E \otimes I_{N^0}] \\ &= \left[I_{N_s} \otimes A^0\right]. \end{aligned} \tag{3}$$

The blocks associated with harmonic coefficients $\delta = 0$ and $\delta = N_s/2$ are simply $\left[A^0\right]$. The blocks associated with the other harmonic coefficients are $\mathrm{diag}(A^0, A^0)$, the rows correspond to the real and the imaginary parts of the Fourier harmonic.

2.2 Multi-stage dynamics

Only multi-stage rotors made of disks whose both geometry and mechanical properties are rotationally periodic are considered here. Such an assembly may be asymmetric, stating that the discrete displacement

defined of the full rotor has no particular property. However, the Fourier transform of its restriction to each disk can be performed.

Consider two disks $\mathcal{D}^1$ and $\mathcal{D}^2$ that are connected through an intermediate ring $\mathcal{R}$ as illustrated by the lumped model in figure 1.

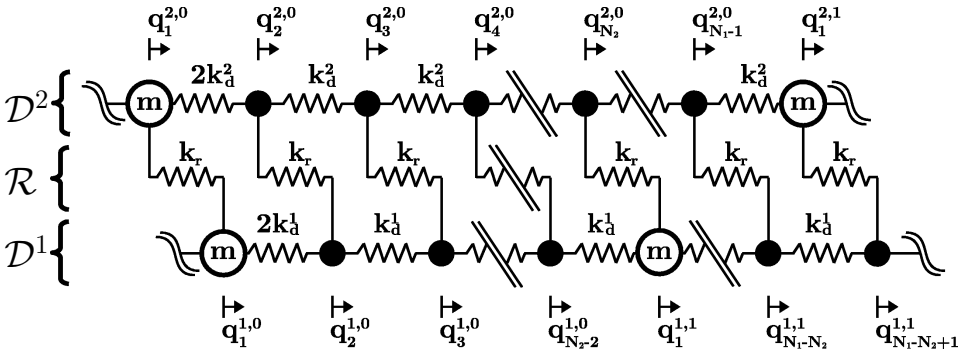

Figure 1: Lumped model of an assembly of tuned disks.

The discrete displacement is

$$\left\{ \begin{array}{c} q^1 \\ q^2 \end{array} \right\} = \left[\begin{array}{cc} E^1 \otimes I_{N^{1,0}} & 0 \\ 0 & E^2 \otimes I_{N^{2,0}} \end{array} \right] \left\{ \begin{array}{c} \widehat{q}^1 \\ \widehat{q}^2 \end{array} \right\}. \tag{4}$$

Any matrix $[A]$ relative to this rotor comes from the assembly of matrices $[A^1]$, $[A^2]$ and $[A^{\mathcal{R}}]$ defined on $\mathcal{D}^1$, $\mathcal{D}^2$ and $\mathcal{R}$ respectively such that

$$[A] = \left[\begin{array}{cc} A^1 & 0 \\ 0 & A^2 \end{array} \right] + \left[A^{\mathcal{R}}\right]. \tag{5}$$

Matrix $[A]$ is transformed into $[\widehat{A}]$

$$[\widehat{A}] = \left[\begin{array}{cc} \widehat{A}^1 & 0 \\ 0 & \widehat{A}^2 \end{array} \right] + [\widehat{A}^{\mathcal{R}}]. \tag{6}$$

Matrices $[\widehat{A}^1]$ and $[\widehat{A}^2]$ are returned by equation (3).

Figure 2 displays matrix $[\widehat{A}^{\mathcal{R}}]$ in the case of two rotors with 4 and 8 sectors and 5 and 8 sectors. It can clearly be seen that in both cases Fourier harmonics are coupled between disks, but remain uncoupled for a given disk, with a simpler pattern when the number of blades are multiples of each other.

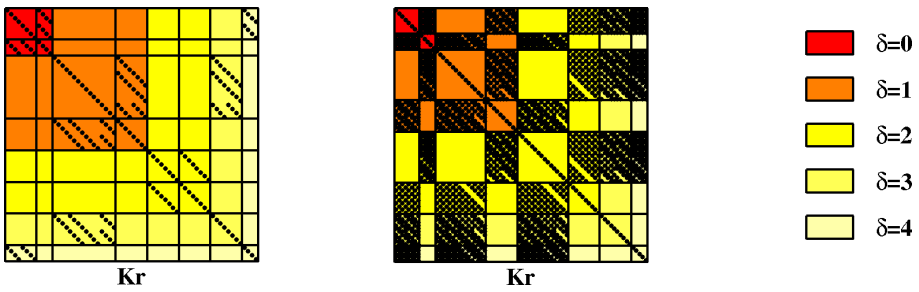

Figure 2: Projected stiffness matrices of the ring for an assembly of disks with 4 and 8 sectors (left) and 5 and 8 sectors (middle). Colormap refers to Fourier harmonics (right).

This figure shows that matrix $[\widehat{A}^{\mathcal{R}}]$ is problematic even if ring $\mathcal{R}$ satisfies cyclic symmetry Fourier harmonics remain coupled. If this matrix is decomposed into blocks indexed by dd' that couple disks $\mathcal{D}^d$ and $\mathcal{D}^{d'}$, these blocks are

$$[\widehat{A}^{\mathcal{R}}_{dd'}] = [E^d \otimes I_{N^{d,0}}]^\top [A^{\mathcal{R}}_{dd'}] [E^{d'} \otimes I_{N^{d',0}}]. \tag{7}$$

These blocks can themselves be subdivided into blocks indexed by $\delta\delta'$ that couple Fourier harmonic $\{q^d_\delta\}$ of $\mathcal{D}^d$ to Fourier harmonic $\{q^{d'}_{\delta'}\}$ of $\mathcal{D}^{d'}$, leading to

$$[\widehat{A}^{\mathcal{R}}_{dd',\delta\delta'}] = [E^d_\delta \otimes I_{N^{d,0}}]^\top [A^{\mathcal{R}}_{dd'}] [E^{d'}_{\delta'} \otimes I_{N^{d',0}}]. \tag{8}$$

Equation (8) shows that:

(i.) the Fourier harmonics of a single disk are not coupled together, thus only mistuning (if any) may contribute to intra-disk harmonic coupling,

(ii.) the Fourier harmonics of given disk are coupled to those of the other disk and is the only contribution to inter-disk harmonic coupling.

The fact that harmonics with different δ are coupled together across the stages prevents a decomposition of the subsequent mechanical problem into mono-harmonic subproblems. Nevertheless, one can assume the inter-disk harmonic coupling to be negligible.

such a decomposition is achieved under the assumption of decoupled harmonics, by selecting in $[\widehat{A}^{\mathcal{R}}]$ only the blocks associated with target coefficient δ. The resulting matrix is denoted $[\widehat{A}^{\mathcal{R}}_\delta]$. From a general dynamic problem formulated for the assembly of disks,

$$[Z]\ \{q\} = \{f\}, \tag{9}$$

with $\{q\} = \{\ q^1 \quad q^2\ \}$ and $\{f\} = \{\ f^1 \quad f^2\ \}$, mono-harmonic solutions are written as

$$\left(\begin{bmatrix} Z^{1,0} & 0 & 0 & 0 \\ 0 & Z^{1,0} & 0 & 0 \\ 0 & 0 & Z^{2,0} & 0 \\ 0 & 0 & 0 & Z^{2,0} \end{bmatrix} + [\widehat{Z}^{\mathcal{R}}_\delta] \right) \begin{Bmatrix} \mathrm{Re}(\widehat{q}^1_\delta) \\ \mathrm{Im}(\widehat{q}^1_\delta) \\ \mathrm{Re}(\widehat{q}^2_\delta) \\ \mathrm{Im}(\widehat{q}^2_\delta) \end{Bmatrix} = \begin{Bmatrix} \mathrm{Re}(\widehat{f}^1_\delta) \\ \mathrm{Im}(\widehat{f}^1_\delta) \\ \mathrm{Re}(\widehat{f}^2_\delta) \\ \mathrm{Im}(\widehat{f}^2_\delta) \end{Bmatrix}, \tag{10}$$

with additional inter-sector continuity conditions that state how the shapes are dephased between two adjacent sectors

$$\begin{bmatrix} c^1_l - \cos(\delta\,\alpha^1)\,c^1_r & \sin(\delta\,\alpha^1)\,c^1_r & 0 & 0 \\ -\sin(\delta\,\alpha^1)\,c^1_r & c^1_l - \cos(\delta\,\alpha^1)\,c^1_r & 0 & 0 \\ 0 & 0 & c^2_l - \cos(\delta\,\alpha^2)\,c^2_r & \sin(\delta\,\alpha^2)\,c^2_r \\ 0 & 0 & -\sin(\delta\,\alpha^2)\,c^2_r & c^2_l - \cos(\delta\,\alpha^2)\,c^2_r \end{bmatrix} \begin{Bmatrix} \mathrm{Re}(\widehat{q}^1_\delta) \\ \mathrm{Im}(\widehat{q}^1_\delta) \\ \mathrm{Re}(\widehat{q}^2_\delta) \\ \mathrm{Im}(\widehat{q}^2_\delta) \end{Bmatrix} = \begin{Bmatrix} 0 \\ 0 \\ 0 \\ 0 \end{Bmatrix}. \tag{11}$$

Particular cases are summarized in table 1 and are exhibited in [7].

Case	$\delta = 0$	$\delta = N^1_s/2$	$\delta = N^2_s/2$	other δ
disk $\mathcal{D}^1$	real	real	complex	complex
disk $\mathcal{D}^2$	real	complex	real	complex

Table 1: Particular cases of equation (10).

Mono-harmonic eigensolutions are derived from equation (10) by letting the right hand terms be zero. One insists on the fact that, in the general case, they are only eigensolutions since they differ from the true eigenmodes of the rotor in the fact that they are mono-harmonic, whereas normal modes are generally multi-harmonic. When at least $\{q^1_\delta\}$ or $\{q^2_\delta\}$ is complex, the projection of the dynamic stiffness matrix of the concerned disk is equivalent to duplicate this matrix. This is unfortunately not the case for the ring, which leads to near-pair eigensolutions. For finer meshes of the ring, the near-pair solutions would converge towards exact pairs.

3 Model reduction

The reduction technique described in this section is a Rayleigh-Ritz method. Such methods generate approximations of the kinematics of the response by combining solutions of simple problems, *e. g.* modes or static shapes. Linear combinations of these are assumed shapes for an approximation subspace. If the initial shapes are not independent a basis generation procedure is needed. The model equations are reduced by a congruent transformation that involves the basis of this subspace. The number of DOFs of the reduced model then corresponds to the subspace dimension.

The proposed method is component based in the sense that the reduction is performed for parts of the structure (in the present case sectors of a disk). The reduced component models are similar to the pair elementary matrix-physical DOFs for a finite element, hence the common denomination of *super-elements*.

In classical Component Mode Synthesis (CMS) [8, 9] one assumes component independence: the reduction basis for a component is obtained by solving static and eigenvalue problems on the component while ignoring others. The fundamental change in the present work is that the reduction bases are generated considering cyclic symmetry solutions.

A classic property of Rayleigh-Ritz methods is that if exact solutions are used to generate the reduction subspace, the reduced model is exact. As detailed in section 2, if cyclic symmetry solutions are exact modes for tuned disks, they are approximate solutions for rotors. Using the restriction of these solutions to sector $\mathcal{S}^{d,s}$ to reduce its model will thus generate a reduced model that will be exact with respect to the retained eigensolutions, approximate for others, thus approximate for the modes of the rotor. Considering classical graphs in which eigenfrequencies are plotted vs. Fourier harmonic coefficients δ (as figure 7 which will be described in section 4.2), one retains the following shapes:

(i.) a set of mono-harmonic solutions $[\ \mathrm{Re}(\Phi^{d,s}_{rcyc})\quad \mathrm{Im}(\Phi^{d,s}_{rcyc})\ ]$ whose harmonics δ are selected for a particular reason (design, ...). These modeshapes are identical for all the sectors of a given disk. They will account for either disk-dominated motion or blade-dominated motion according to their position in the graph $f(\delta)$,

(ii.) if needed, a set of eigenmodes $[\Phi^{d,s}_{fix}]$ of this sector with its left and right interfaces both clamped. These modes can differ from a sector to another. They will account for blade-dominated motion. High δ shapes will however be nearly identical to such shapes.

The initial set of assumed vectors considered to generate the reduction will thus always be of the form

$$[T^{d,s}_{init}] = [\ \mathrm{Re}(\Phi^{d,s}_{rcyc})\quad \mathrm{Im}(\Phi^{d,s}_{rcyc})\quad \Phi^{d,s}_{fix}\ ]. \tag{12}$$

A first difficulty is that such sets of vectors are often degenerate. A trivial case of dependence is found if one retains both modes of pairs found for $\delta > 0$, since it is known that the second model can be found by shifting the Fourier transform of the modeshape. Less obvious cases are found when retaining vectors from multiple δ. The independence of vectors may then be lost for the considered numerical precision. Methods to deal with this problem are discussed in section 3.1.

A second difficulty is that coupling of components within a Rayleigh-Ritz procedure requires the assumed shapes to be continuous (kinematically admissible). A first method, described in [10], takes a basis of subspace generated by $[T^{d,s}_{init}]$ and completes it to obtain left and right generalized DOFs whose equality across sector interfaces implies continuity at all points of the unreduced model. The proposed method described in section 3.2 completely bypasses the difficulty of enforcing continuity by considering reduced models that are disjoint. Components are then coupled by reducing the model of an interface rather than enforcing inter-component continuity.

3.1 Assumed vectors and reduction bases

In the considered applications, one uses reference computations to generate sets of assumed shapes. When keeping modes of multiple target Fourier coefficients, the sets of generating vectors kept in $[T_{init}^{d,s}]$ are not bases in the sense that they are not full rank. Using non full rank reduction bases generates models that are singular or at least poorly conditioned. Procedures to generate bases from large vector sets are thus critical for the proposed reduction methods.

In linear algebra, the classical approach to generate a well conditioned basis for a subspace is to generate an orthonormal basis of that subspace. The key issues in the process are the way to guarantee orthogonality in the presence of numerical round-off errors and the criterion used to eliminate dependent vectors.

The singular value decomposition (see [11] for example) is the most robust approach to generate an orthonormal basis. Using a Euclidean norm (norm $||.||_2$) on a vector of degrees of freedom is however not particularly suited for applications in mechanics. It was shown in [12] that solving for the lowest frequency eigenvalues of the reduced mass and stiffness matrices gives a proper extension of the singular value decomposition to mechanics. The result of the decomposition is of the form

$$[T] = [U][\Sigma][V]^T \tag{13}$$

where $[\Sigma]$ is diagonal and ranks the contributions of the orthonormal vectors in $[U]$. A basis of the subspace is thus obtained by keeping the columns $\{U_j\}$ corresponding to significant singular values (such that $\sigma_j \geqslant \epsilon\, \sigma_1$).

A proper use of the SVD requires that the columns of $[T]$ to have comparable initial scaling. This is typically achieved by initial scaling of each of the columns. In the proposed applications, the bases are composed of modes that are typically mass normalized. No rescaling is thus needed.

Gram-Schmidt methods (see annex 2 of [13] for example) provide a classical procedure to generate a basis from a set of vectors. They are however very sensitive to numerical round-off. Modified Gram-Schmidt methods do a recursive orthogonalization which alleviates the numerical problem but do not introduce a mechanism to eliminate vectors. Iterative modified Gram-Schmidt (IMGS) provides a procedure that gives a robust mechanism to eliminate vectors that are not independent.

In Gram-Schmidt methods, vectors are considered dependent if the norm of the part orthogonal to currently retained vectors is too small. Practically if $\{\widehat{T}_j\}$ is the part of $\{T_j\}$ orthogonal to $\{T_k\}$ with $k < j$, the vector is truncated if $||\widehat{T}_j||_2 < \epsilon\, ||T_j||_2$.

The use of orthonormal bases in both SVD and Gram-Schmidt methods is motivated by the need to guarantee the independence of base vectors. An other approach to achieve the same result is to ensure that each vector is non zero at a different location. This is the classical approach of finite element models where shape functions are equal to one at the location associated to their DOF and zero at the locations of other DOFs. This idea motivated the Independent Maximum Sequence (IMS) algorithm presented in [14] for sensor placement and used here to generate bases.

The IMS algorithm iteratively defines a series of independent vectors generating the target subspace as follows. At step i,

- one seeks for vector $\{T_i\}$ the value of DOF m with maximum absolute amplitude. If this amplitude is too small (a typical value of $10^{-8} \times \max(T_0)$), the vector is eliminated.
- the vector is normalized in the sense of norm $||.||_\infty$

$$\{\widetilde{T}_i\} = \frac{\{T_i\}}{T_i(m)} = \frac{\{T_i\}}{||T_i||_\infty},$$

- further vectors $\{T_j\}$ with $j > i$ are made independent from $\{T_i\}$ by making the response at DOF m equal to zero (psychologically orthogonal)

$$\{\widetilde{T}_j\} = \{T_j\} - \{\widetilde{T}_i\}\, T_j(m).$$

This step is not an orthogonalization but guarantees independence too.

This procedure generates vectors that are obviously independent (the maximum of $\{T_j\}$ is is reached at a position where $T_j = 0$ for $j > i$) and normalized (the maximum of all vectors is 1). The elimination mechanism is well suited if the initial vectors are scaled in a similar fashion, as is the case in the proposed methods where the generating vectors are mass normalized modes. The cost of finding the maximum response is much lower than that of computing a scalar product, the procedure thus costs significantly less than Gram-Schmidt methods and does not require any iteration for round-off problems.

A significant motivation for the use of the IMS algorithm in this work is its ability to generate bases that are strictly zero on a subset of DOFs. The procedure is as follows. Let the DOFs be partitioned in two sets a and b. The modified IMS algorithm proceeds iteratively in three phases. One first reorders vectors by the maximum amplitude within DOF set a. One the selects a basis of the restriction of $\{T\}$ to DOF set a. To do so, at step i,

- one seeks for vector T_i the value of the DOFs m with maximum absolute amplitude within DOF set a.
- if $||T_i||_\infty < \epsilon_1 ||T_0||_\infty$ the vector is considered dependent and eliminated: linear combinations with vectors of lower index led to a null vector.
- if $T_i(m) < \epsilon_2 ||T_i||_\infty$ the vector is considered null within set a. $\{T_{i,a}\}$ is set strictly to $\{0\}$ and the vector is set aside for the third phase.
- further vectors $\{T_j\}$ with $j > i$ are made independent from $\{T_i\}$ by making the response at DOF m equal to zero
$$\{\widehat{T}_j\} = \{T_j\} - \{\widehat{T}_i\}\, T_j(m).$$

In the last phase, vectors set aside as having a strictly null contribution on DOF set a can be made independent using the classical IMS approach.

The procedure thus generates a basis which guarantees vectors independence by the means of blocks of zeros. Like all methods with elimination, the results are somewhat dependent on the tolerances (values ϵ_i). While the issue should be considered in further detail, the results presented use $\epsilon_1 = 10^{-8}$ and $\epsilon_2 = 10^{-4}$.

3.2 Definition of the super-elements

When it comes to multi-stage assemblies, sectors of a given disk are not only connected to each other, but also with one or more sectors that belong to the adjacent disks, through a volumic interface in the present method. Figure 3a displays the sample academic rotor used in [7] with some updates. Table 2 summarizes the characteristics of its mesh.

Stage	Nb. of sectors	Nb. of Nodes/sec.	Nb. of Elements/sec.	Nb. of DOFs/sec.	Type of Elements
1	12	184	84	552	Hexa8
2	15	184	84	552	Hexa8

Table 2: Description of the finite element model of the sectors of the academic rotor.

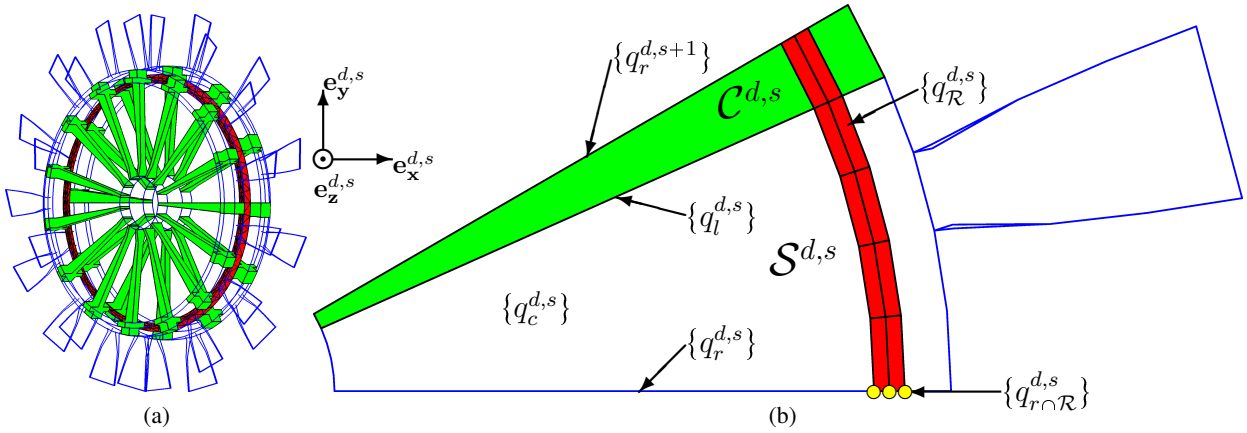

Figure 3: Sector substructuring in the multi-disk case: (□) sector super-element, (■) inter-sector super-element and (■) ring surface.

Each bladed sector is condensed into an sector super-element (white region with blue border in figure 3) that is connected thanks to inter-sector slices, themselves condensed into a super-element for convenience (green region with black border in figure 3) and inter-disk rings $\mathcal{R}$ that are kept as is (red region in figure 3). The discrete displacement of sector $\mathcal{S}^{d,s}$ is partitioned according to figure 3b so that

$$\{q^{d,s}\}^\top = \left\{ \begin{array}{ccccc} q_{r\cap\mathcal{R}}^{d,s} & q_r^{d,s} & q_\mathcal{R}^{d,s} & q_c^{d,s} & q_l^{d,s} \end{array} \right\}. \tag{14}$$

The approximate kinematic subspace of sector $\mathcal{S}^{d,s}$ is built so that $\{q^{d,s}\}$ is sought in this subspace as

$$\{q^{d,s}\} = [T_M^{d,s}]\,\{q_M^{d,s}\}, \tag{15}$$

where $\{q_M^{d,s}\}$ contains the generalized degrees of freedom. $[T_M^{d,s}]$ is a basis of the subspace derived from $[T_{init}^{d,s}]$, which is partitioned according to equation (14) into

$$[T_M^{d,s}]^\top = \left[\begin{array}{ccccc} T_{M,r\cap\mathcal{R}}^{d,s} & T_{M,r}^{d,s} & T_{M,\mathcal{R}}^{d,s} & T_{M,c}^{d,s} & T_{M,l}^{d,s} \end{array} \right]. \tag{16}$$

Any matrix $[A^{d,s}]$ relative to sector $\mathcal{S}^{d,s}$ is then projected onto the subspace spanned by $[T_M^{d,s}]$ thanks to the relation

$$[A_M^{d,s}] = [{T_M^{d,s}}^\top\, A^{d,s}\, T_M^{d,s}]. \tag{17}$$

According to equation (14), slice $\mathcal{C}^{d,s}$ that connects sectors $\mathcal{S}^{d,s}$ and $\mathcal{S}^{d,s+1}$ couple $\{q_l^{d,s}\}$ to $\{q_{r\cap\mathcal{R}}^{d,s+1}\}$ and $\{q_r^{d,s+1}\}$, so that any matrix $[A_\mathcal{C}^{d,s}]$ relative to this slice has to be projected on the subspace generated by $[T_{M,l}^{d,s}]$, $[T_{M,r\cap\mathcal{R}}^{d,s+1}]$ and $[T_{M,r}^{d,s+1}]$ such that

$$[A_{M,\mathcal{C}}^{d,s}] = \left[\begin{array}{cc} T_{M,l}^{d,s} & 0 \\ 0 & T_{M,r\cap\mathcal{R}}^{d,s+1} \\ 0 & T_{M,r}^{d,s+1} \end{array} \right]^\top [A_\mathcal{C}^{d,s}] \left[\begin{array}{cc} T_{M,l}^{d,s} & 0 \\ 0 & T_{M,r\cap\mathcal{R}}^{d,s+1} \\ 0 & T_{M,r}^{d,s+1} \end{array} \right]. \tag{18}$$

Ring $\mathcal{R}$ between disks $\mathcal{D}^d$ and $\mathcal{D}^{d'}$ connects $\{q_{r\cap\mathcal{R}}^{d,s}\}$ and $\{q_\mathcal{R}^{d,s}\}$, $\forall s \in [\![0, N_s^d - 1]\!]$, to $\{q_{r\cap\mathcal{R}}^{d',s'}\}$ and $\{q_\mathcal{R}^{d',s'}\}$, $\forall s' \in [\![0, N_s^{d'} - 1]\!]$. Any matrix $[A^\mathcal{R}]$ relative to ring $\mathcal{R}$ is projected on the full subspace spanned by the vectors in the restriction of $[T_M]$ to the ring DOFs denoted $[T_{M,\mathcal{R}}]$ (not shown here for the sake of brevity)

$$[A_{M,\mathcal{R}}^\mathcal{R}] = [T_{M,\mathcal{R}}^\top\, A^\mathcal{R}\, T_{M,\mathcal{R}}]. \tag{19}$$

To limit connectivity and guarantee vector independence, one chose to build a basis with the following target topology

$$[T_M^{d,s}] = \begin{bmatrix} \widetilde{T}^{d,s}_{M,r\cap\mathcal{R},r\cap\mathcal{R}} & 0 & 0 & 0 \\ \widetilde{T}^{d,s}_{M,r,r\cap\mathcal{R}} & \widetilde{T}^{d,s}_{M,r,r} & 0 & 0 \\ \widetilde{T}^{d,s}_{M,\mathcal{R},r\cap\mathcal{R}} & 0 & \widetilde{T}^{d,s}_{M,\mathcal{R},\mathcal{R}} & 0 \\ \widetilde{T}^{d,s}_{M,c,r\cap\mathcal{R}} & \widetilde{T}^{d,s}_{M,c,r} & 0 & \widetilde{T}^{d,s}_{M,c,c} \\ \widetilde{T}^{d,s}_{M,l,r\cap\mathcal{R}} & \widetilde{T}^{d,s}_{M,l,r} & 0 & \widetilde{T}^{d,s}_{M,l,c} \end{bmatrix}. \tag{20}$$

In this basis one distinguishes

- $[\widetilde{T}^{d,s}_{M,r\cap\mathcal{R}}]$ non zero shapes that have their maximum on DOFs common to the right edge r and the rings $\mathcal{R}$. These are in very limited number and thus kept non-zero everywhere. They are selected by a sort of the initial vectors by contribution on the $r \cap \mathcal{R}$ DOF set followed by simple application of the IMS algorithm.
- $[\widetilde{T}^{d,s}_{M,r\cap\mathcal{R}}]$ shapes that are only zero on the right edge/ring intersection $r \cap \mathcal{R}$. They are obtained by simple application of the IMS algorithm on the remaining vectors.
- other shapes are possibly non zero on both the interior c and ring DOFs. To limit coupling, one builds $[\widetilde{T}^{d,s}_{M,\mathcal{R},\mathcal{R}}]$ by singular value decomposition of the trace on $\mathcal{R}$ of the remaining vectors and $[\widetilde{T}^{d,s}_{M,r}]$ by application of the IMS for the trace of the same vectors on $c \cup l$. This step thus involves some replication, which was deemed acceptable.

Figure 4 displays the transpose of a sample multi-disk reduction basis for disk $\mathcal{D}^1$ with vector ordering (not used but shown here for legibility). The triangular areas of non-zero data in this figure correspond to typical results of the IMS.

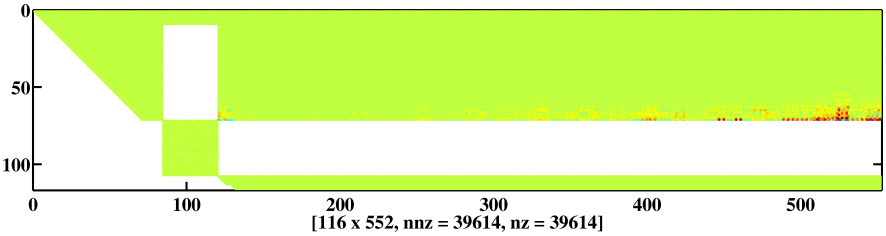

Figure 4: Sample multi-stage reduction basis of a single sector with vectors sorted.

Note that the full subspace of motion of the rotor is never explicitly built but the reduced matrices are assembled from the super-elementary matrices in two steps:

Step 1: the physical finite element matrices of the sectors and inter-sector matrices are built sector by sector, disk by disk, thanks to Eqns. (17) and (18), leading to matrices $[A_M^{d,s}]$ and $[A_{M,C}^{d,s}]$ associated to sector $\mathcal{S}^{d,s}$ and inter-sector slice $\mathcal{C}^{d,s}$ respectively. These matrices are assembled into reduced disk matrices, exactly as in the mono-disk approach.

Step 2: the matrices of the ring are projected onto the kinematic subspaces of its neighbouring disks with respect to the inter-disk generalized DOFs thanks to equation (19). In order to avoid using the basis of the full subspace, $[A_M^{\mathcal{R}}]$ is built iteratively block by block, *i. e.* sector by sector.

A typical matrix topology is displayed in figure 5, where it can be seen that the bandwidth of such matrices is quite wide, leading to large factorized matrices.

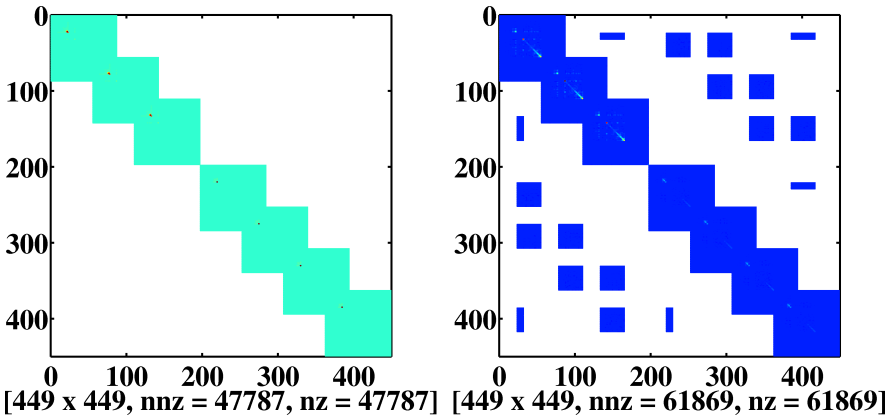

Figure 5: Topology of the reduced matrices: (left) without ring coupling and (right) with ring coupling.

4 Application to an industrial rotor

4.1 Presentation of the model

The numerical model of a compressor in development was used as an illustration. It is depicted in figure 6 and is composed of three integrally bladed disks (blisks), whose characteristics are reported in Tab. 3. The full finite element model is made of $11,289,230$ tetrahedrons connecting $2,631,094$ nodes, with a total of $7,893,282$ DOFs. Only linear elements are used here, but computations with quadratic elements are currently in progress.

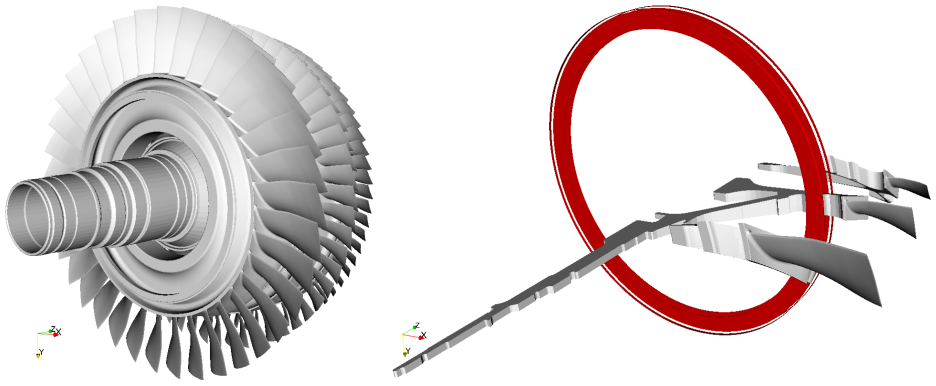

(a) (b)

Figure 6: Industrial 3 stage HP compressor: (a) full model and (b) sector model.

Stage	Nb. of sectors	Nb. of Nodes/sec.	Nb. of Elements/sec.	Nb. of DOFs/sec.	Type of Elements
1	36	$16,343$	$65,170$	$49,029$	Tetra4
2	56	$9,566$	$36,815$	$28,698$	Tetra4
3	70	$23,104$	$97,860$	$69,312$	Tetra4

Table 3: Finite element model of the 3 blisks of the HP compressor with linear elements.

4.2 Mono-harmonic modeshapes

Figure 6b focuses on the sector plus ring model that is used for mono-harmonic computations. The full graph that displays the eigenfrequencies of the rotor and the disks with various boundary conditions is depicted in figure 7. Frequencies normalized with respect to the frequency of the first flexible 0 diameter solution of the rotor are denoted by f.

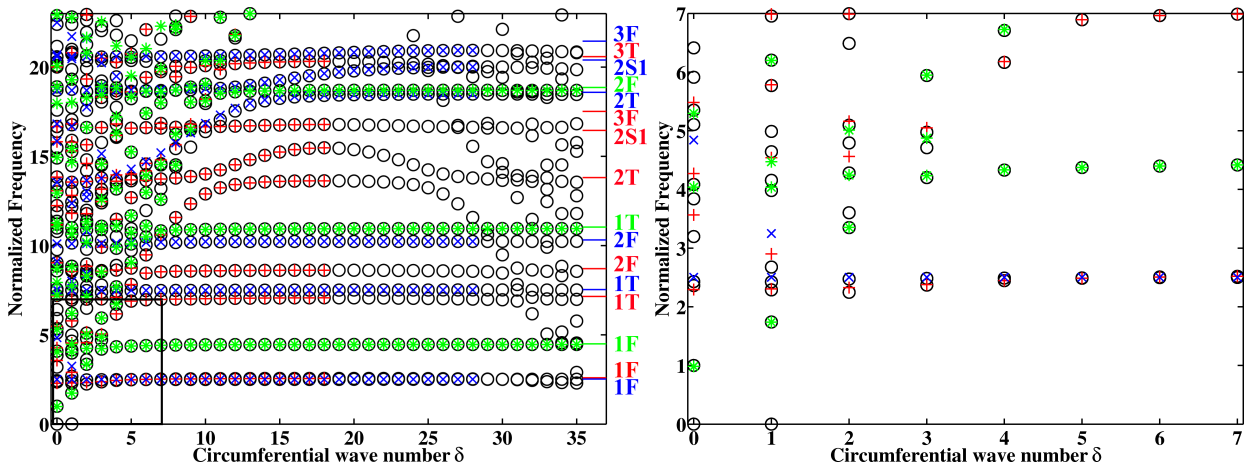

Figure 7: (a) Full and (b) zoomed normalized frequencies of the cyclic solutions for the rotor (◯) and the modes of disk $\mathcal{D}^1$ (+), disk $\mathcal{D}^2$ (×) and disk $\mathcal{D}^3$ (✳) in free-fix, fix-fix and fix-free condition. (—), (—) and (—) are asymptotic blade mode frequency.

It can be seen that all coupled solutions lie inside a triangle that has $\delta = 0, f = 0$ as a summit, and $\delta = 0$ and $f = \delta$ as edges, with a replication of such triangle with respect to $\delta = 15$ du to aliasing. In this area, as Fourier harmonic coefficient δ increases, noticeable differences between the frequencies of the rotor solutions and the disk natural frequencies are observed, due to the fact that a fix condition at inter-stage interfaces is too stiff and disk modes that are similar to solutions of the rotor are higher in frequency, as can be seen in the zoomed region in figure 7b. On the contrary, modes of the disks with free rims would be below rotor solutions since a free condition at the inter-stage interfaces is far too soft. Elsewhere, many mono-harmonic solutions are close to modes of the individual disks, merely due to:

(i.) a small disk-blade coupling, which confines the strain energy on the blades [2]. The motion similar to that of the individual disks whatever their boundary conditions, because the latter do not affect the blade-dominated motion due to the low coupling ratio between the disk and the blades.

(ii.) a small disk-disk coupling, which confines the strain energy on a single disk.

Typical mono-harmonic solutions are exhibited in figure 8, they can involve either a single disk or many disk, which implies that the extended cyclic symmetric model correctly takes inter-disk coupling into account.

4.3 Reduced model

The reduced model is built from a set of cyclic solutions with $\delta \in \{0, 2\}$ and $f \in [0, 16.13]$. $44,342$ generalized DOFs were involved after the reduction process. The assembled reduced stiffness matrix occupies 1022 Mb before and 16 Gb after factorization.

The generalized modes in the normalized frequency range $[0, 19.5]$ were computed. A Fourier transform of the reduced modeshapes was performed so that the spatial spectrum of the generalized modes could be exhibited

per disk. As displayed in figures 9 and 10, localized multi-harmonic modes and coupled mono-harmonic modes were found.

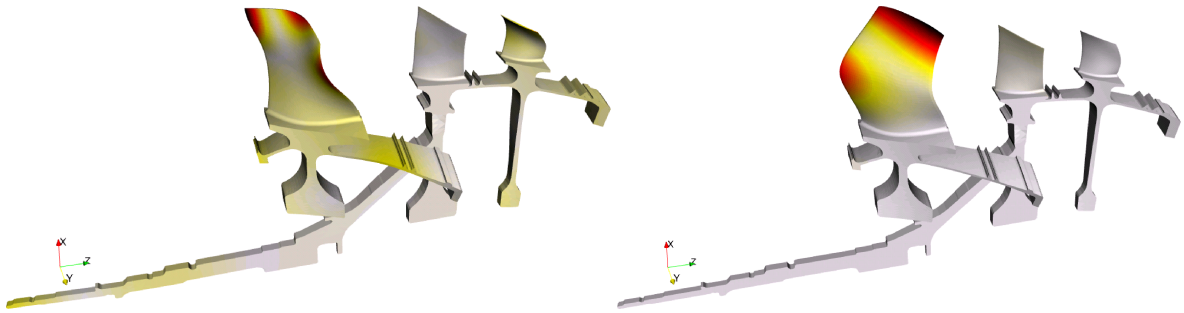

(a) (b)

Figure 8: (a) Coupled cyclic solution with $\delta = 1$ at $f = 15.53$ (blade shapes are 2S1, 2F and 1T) and (b) cyclic solution localized to disk $\mathcal{D}^1$ with $\delta = 4$ at $f = 8.63$ (blade shape is 2F).

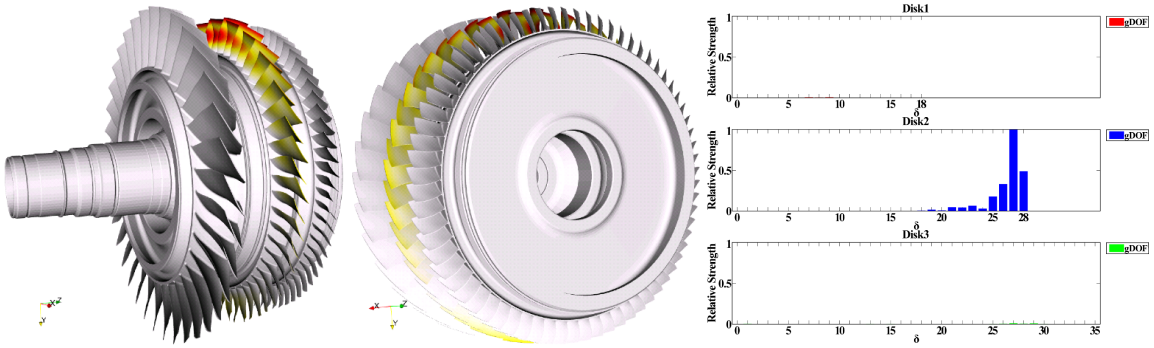

(a) (b)

Figure 9: Restored mode at $f = 10.23$ localized to disk $\mathcal{D}^2$: (a) modeshape and (b) spatial harmonic content for disks (■) $\mathcal{D}^1$, (■) $\mathcal{D}^2$ and (■) $\mathcal{D}^3$.

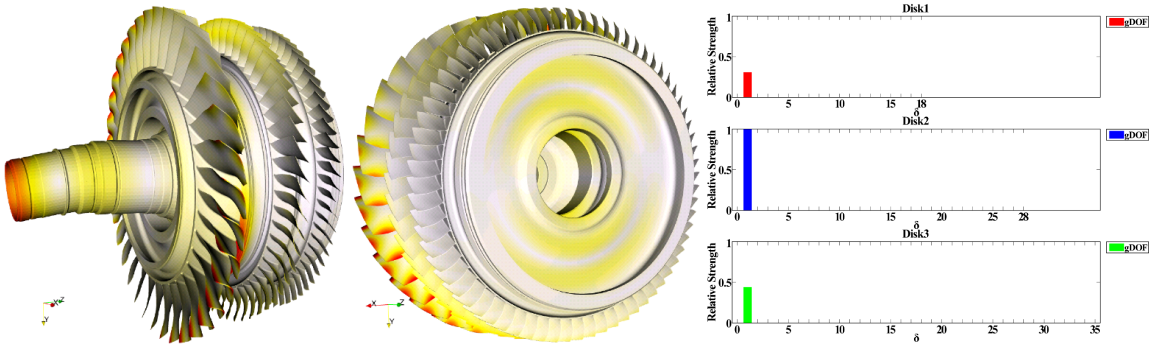

(a) (b)

Figure 10: Restored mode at $f = 15.89$ with strong coupling: (a) modeshape and (b) spatial harmonic content for disks (■) $\mathcal{D}^1$, (■) $\mathcal{D}^2$ and (■) $\mathcal{D}^3$.

4.4 Recovery

Using equation (15) the full displacement can be recovered sector by sector. However, the finite element model described in table 3 cannot easily be displayed and manipulated. Moreover, the full recovery of the modeshapes as exhibited in figures 9a and 10a may not be necessary when the motion is localized to a limited area. A subset γ of physical DOFs can be chosen for each sector $\mathcal{S}^{d,s}$ so that the motion is recovered to this subset only thanks to

$$\{q_\gamma^{d,s}\} = [T_{M,\gamma}^{d,s}]\,\{q_M^{d,s}\}, \tag{21}$$

where $[T_{M,\gamma}^{d,s}]$ is the restriction of $[T_M^{d,s}]$ to subset γ. This subset can be different from a sector to another and can be different from the finite element mesh of the rotor. Two typical choices are displayed in figure 11 and are:

- a pseudo-mesh that leans on nodes of the finite element model, connected by display only elements. This gives only a quick insight into the motion, but allows to determine what kind of blade motion is involved. Nevertheless, it provides a wireframe to perform test/analysis correlation.
- a subset of finite elements, which can be used for strain, stress and energy post-processing.

Both are applicable to recovery of cyclic symmetry modeshapes, as it is done in figure 11a for an eigensolution with $\delta = 1$, as well as reduced computations as it is done in figure 11b for a reduced mode with $f = 15.89$ whose Von Mises stress is computed for a few elements of disk $\mathcal{D}^1$. The subset of finite elements used to post-process this mode was selected from the recovery of the motion on the same pseudo-mesh as in figure 11a, noticing that both the tips of the blades in $\mathcal{D}^1$ and the rim between disks $\mathcal{D}^1$ and $\mathcal{D}^2$ had a motion with a high amplitude for this generalized mode.

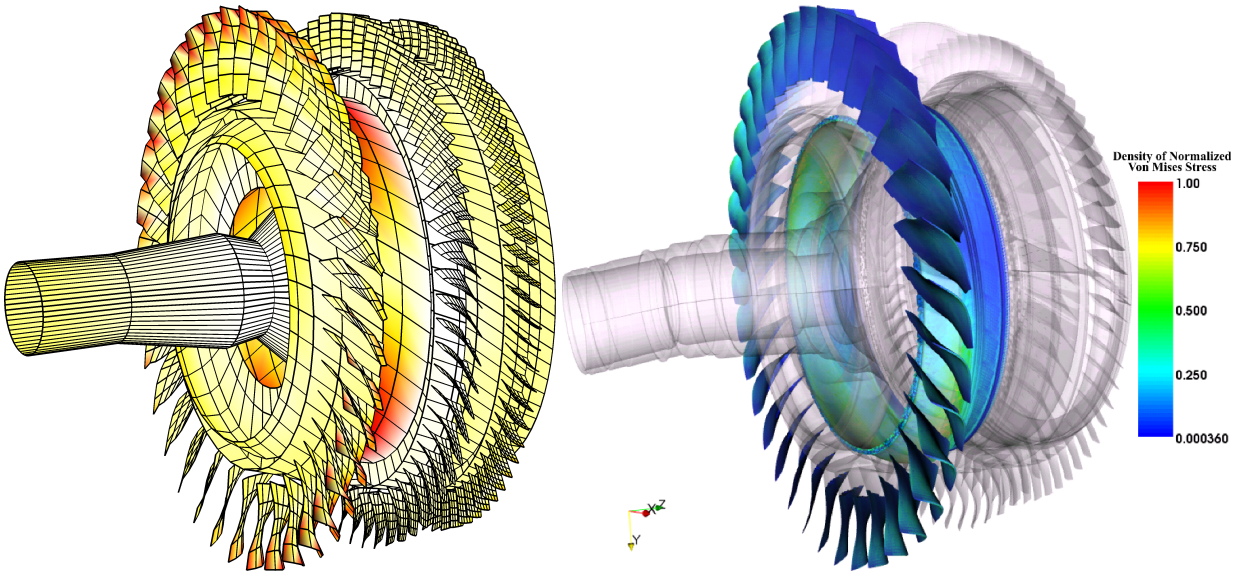

(a) (b)

Figure 11: Partial recovery of (a) motion and (b) stresses.

5 Conclusions

The present paper introduces a multi-stage reduction technique the authors developed and presents its application to an industrial rotor model. Guidelines for an effective use of the proposed method are derived from this study:

(i.) a set of mono-harmonic solutions are computed, they contain valuable information in the sense that a direct interpretation can be performed,

(ii.) this set is used to build a compact reduced model that represents the multi-stage model with a controlled accuracy, with subsequent enrichments of the kinematic spaces if requested (such strategies are the object of future work).

(iii.) when the Fourier transform of modes show that they are spatially mono-harmonic, they can be paired to mono-harmonic solutions. In such case, if the excitation is a single engine-order, the forced response can be computed directly from the mono-harmonic subproblems.

(iv.) if some of the modes of interest are multi-harmonic, they may be forced by any external excitation and the response must be computed with the reduced model.

(v.) in every case, a subset of true or display elements can be chosen for partial recovery. This choice is driven either by an *a priori* analysis of the mono-harmonic solutions or by an *a posteriori* analysis of the spatial spectrum of the generalized modes.

This methodology is implemented within the Structural Dynamics Toolbox [15] with critical use of the super-element capabilities of this library. Internal element formulations are used although imports from SAMCEF and NASTRAN have also been done for verification. The SDT switches to use NASTRAN as the eigenvalue solver for SDT based models when models become very large. The SDT/OpenFEM export to VTK format was used to generate some of the figures included in this paper with ParaView. Developments specific to this study, grouped as the embryo of an SDT/Rotor package, are

(i.) pre-processing tools to assemble sector models and mesh rings using an automated volume mesher,

(ii.) mono-harmonic rotor computations,

(iii.) sector super-element building from a set of mono-harmonic multi-stage solutions and fixed sector modes,

(iv.) post-processing tools for harmonic and generalized coordinate viewing.

Acknowledgments

Thanks go to Snecma for its technical and financial support. This work takes place in the framework of the MAIA mechanical research and technology program sponsored by CNRS, ONERA and SAFRAN Group.

References

[1] A. V. Srinivasan. Flutter and Resonant Vibration Characteristics of Engine Blades. *ASME Journal of Engineering for Gas Turbines and Power*, 119:742–775, 1997.

[2] M. P. Castanier and C. Pierre. Modeling and Analysis of Mistuned Bladed Disk Vibration: Status and Emerging Directions. *Journal of Propulsion and Power*, 22(2):384–396, 2006.

[3] R. Bladh, M. P. Castanier, and C. Pierre. Effects of Multistage Coupling and Disk Flexibility on Mistuned Bladed Disk Dynamics. *ASME Journal of Engineering for Gas Turbines and Power*, 125:121–130, 2003.

[4] A. Sternchüss and E. Balmès. Reduction of Multistage Rotor Models Through Cyclic Modeshapes. In *Proceedings of ASME Turbo Expo, Montréal, Canada*, 2007. Paper Number GT2007-27974.

[5] S. H. Song, M. P. Castanier, and C. Pierre. System Identification of Multistage Turbine Engine Rotors. In *Proceedings of ASME Turbo Expo, Montréal, Canada*, 2007. Paper Number GT2007-28307.

[6] D. Laxalde, J.-P. Lombard, and F. Thouverez. Dynamics of Multi-Stage Bladed Disk Systems. In *Proceedings of ASME Turbo Expo, Montréal, Canada*, 2007. Paper Number GT2007-27083.

[7] A. Sternchüss, E. Balmès, P. Jean, and J.-P. Lombard. Reduction of multi-stage disk models: Application to an industrial rotor. *ASME Journal of Engineering for Gas Turbines and Power*. To appear.

[8] R. Jr. Craig. A review of time-domain and frequency domain component mode synthesis methods. *Int. J. Anal. and Exp. Modal Analysis*, 2(2):59–72, 1987.

[9] M. Géradin and D. Rixen. *Mechanical Vibrations. Theory and Application to Structural Dynamics.* John Wiley & Wiley and Sons, 1994, also in French, Masson, Paris, 1993.

[10] A. Sternchüss and E. Balmès. On the reduction of quasi-cyclic disks with variable rotation speeds. In *Proceedings of the International Conference on Advanced Acoustics and Vibration Engineering (ISMA)*, pages 3925–3939, 2006.

[11] G.H. Golub and C.F. Van Loan. *Matrix computations*. Johns Hopkins University Press, 1983.

[12] E. Balmès. Optimal ritz vectors for component mode synthesis using the singular value decomposition. *AIAA Journal*, 34(6):1256–1260, 1996.

[13] O. Boiteau. *Algorithme de résolution pour le problème généralisé*. Code Aster, EDF Recherche et Développement, Clamart. R5.01.01-C.

[14] E. Balmès. Orthogonal Maximum Sequence Sensor Placements Algorithms for modal tests, expansion and visibility. *International Modal Analysis Conference*, 2005.

[15] E. Balmès, J.-P. Bianchi, and J.-M. Leclère. *Structural Dynamics Toolbox 6.0 (for use with MATLAB)*. SDTools, Paris, France, 2007.